Nanoscale

PAPER

View Article Online
View Journal | View Issue

Check for updates

Cite this: *Nanoscale*, 2025, **17**, 26738

Understanding the interfacial interaction characteristics of asphalt nanocomposites reinforced with diamond nanothreads and carbon nanotubes

Fenghua Nie, [a,b] Hang Lin,[a] Xing Su,[a] Qifan Ren,[a] Xuefeng Liu*[b,c] and Ke Ou[d]

Diamond nanothreads (DNTs) and carbon nanotubes (CNTs) have emerged as promising reinforcement materials for asphalt. However, the interfacial properties between DNTs/CNTs and asphalt remain poorly understood, hindering the advancement of DNT-/CNT-modified asphalt nanocomposites. In this study, pullout tests were conducted on asphalt nanocomposites reinforced with DNTs, nitrogen-doped diamond nanothreads (NDNTs), and CNTs, to analyze the pullout performance and reinforcing mechanisms across various temperature ranges. The findings reveal that CNT-modified asphalt nanocomposites exhibited superior pullout performance compared to those reinforced with DNTs, primarily due to π–π stacking interactions that facilitated the wrapping of asphalt molecules around CNT surfaces. Among the DNT variants, the DNT2-modified asphalt nanocomposite demonstrated the highest pullout performance, which was attributed to its helical structure that enhanced mechanical interlocking within the asphalt matrix. Notably, NDNTs showed the highest binding energy relative to DNTs and CNTs, stemming from interactions between hydroxyl groups on asphaltene-phenol and nitrogen atoms on NDNTs, leading to the formation of O–H···N hydrogen bonds. Density functional theory (DFT) calculations indicated that nitrogen doping modified the electronic structure of NDNTs, resulting in localized negative charges that enhance their overall electronegativity.

Received 12th August 2025,
Accepted 21st October 2025

DOI: 10.1039/d5nr03427b

rsc.li/nanoscale

Open Access Article. Published on 28 October 2025. Downloaded on 5/1/2026 11:16:17 PM.
This article is licensed under a Creative Commons Attribution-NonCommercial 3.0 Unported Licence.

1 Introduction

1.1 Background

While asphalt pavements offer advantages such as smooth and quiet surfaces, rapid construction, and simplified maintenance, their widespread application is constrained by the inherent thermomechanical properties of asphalt.[1] The thermomechanical properties of asphalt refer to how its mechanical behavior changes in response to temperature variations.[2,3] Poor thermomechanical properties lead to temperature-induced distress and fatigue cracking under loads and environmental impacts, necessitating frequent and costly maintenance that strains infrastructure budgets and disrupts traffic. Therefore, it is imperative to improve the thermomechanical properties of asphalt through innovative material modification strategies to enhance the long-term durability of asphalt pavement.

1.2 Literature review

Various modification methods have been developed over the past few decades to enhance the thermomechanical properties of asphalt.[4] Early approaches primarily focused on incorporating polymers, such as styrene–butadiene–styrene (SBS) and crumb rubber (CRM), to improve asphalt's performance.[5] SBS enhances high-temperature performance and deformation resistance, while CRM improves low-temperature performance and reduces noise pollution.[6] However, polymer modifiers are vulnerable to environmental factors such as heat, oxygen, and ultraviolet (UV) radiation, which can compromise the long-term performance of modified asphalt composites. Additionally, fiber reinforcement—utilizing cellulose fibers, mineral fibers, and synthetic fibers—can significantly enhance tensile strength and fatigue resistance by creating a reinforcing network within the asphalt.[7,8] However, fibers often tend to accumulate and clump during the mixing process, resulting in uneven distribution and compromised performance of the final composite material.

[a]*School of Resources and Safety Engineering, Central South University, Changsha, China*
[b]*Department of Architecture and Civil Engineering, City University of Hong Kong, Hong Kong, China. E-mail: xfliu6-c@my.cityu.edu.hk*
[c]*College of Hydraulic and Environmental Engineering, China Three Gorges University, Yichang, China*
[d]*China Railway No. 5 Engineering Group Co. Ltd, China*

This journal is © The Royal Society of Chemistry 2025

Open Access Article. Published on 28 October 2025. Downloaded on 5/1/2026 11:16:17 PM. This article is licensed under a Creative Commons Attribution-NonCommercial 3.0 Unported Licence.

There are limitations to traditional modification methods, but the introduction of nanomaterials offers a promising alternative. Because the unique physical and chemical properties of nanomaterials provide significant advantages in enhancing the performance of asphalt, they are an attractive option for future research and application.[9] Nanomaterials, particularly carbon-based materials such as carbon nanotubes (CNTs) and graphene, as well as inorganic materials such as nano-clay, nano-silica, and nano-TiO_2, exhibit exceptional mechanical properties, high specific surface areas, and excellent thermal stability. These characteristics enable these specific nanomaterials to significantly enhance the thermo-mechanical properties of asphalt. It has been demonstrated that the incorporation of CNTs, graphene, and other nanomaterials can lead to improvements in the stiffness, deformation resistance, fatigue cracking resistance, and self-healing properties of asphalt.[10–12] The significant surface area of nanomaterials facilitates strong adsorption and interaction with asphalt molecules, leading to the formation of homogeneous and stable nanocomposite structures.[13] Moreover, the enhanced interaction facilitates the load transfer and stress distribution within the asphalt, resulting in increased toughness and resistance against deformation and cracking.

Diamond nanothread (DNT) is a particularly intriguing option due to its predicted exceptional tensile strength, stiffness, and unique surface chemistry.[14] With remarkable mechanical properties, DNT possesses a Young's modulus of 850 GPa and bending rigidity of 5.38×10^{-28} N m^{-2}. DNTs exhibit a significantly higher torsional elastic limit (almost three times greater) and interfacial load transfer (more than double) compared to CNTs.[15] Their thermal expansion coefficient is low, and they possess remarkable thermal stability, demonstrating negligible thermal deformation and degradation during temperature fluctuations.[16] Their thermal conductivity can reach up to 2000 W m^{-1} K^{-1}, which facilitates an even distribution of pavement temperature. This, in turn, assists in minimizing thermal stress concentrations and lowers the risk of cold cracking of asphalt. Furthermore, the hydrogenated surfaces facilitate covalent bonding between DNTs and the matrix, allowing for their functionalization without introducing any defect in the backbone structure so that they are especially suitable as modifiers for nanocomposites.[17,18]

In particular, nitrogen-doped diamond nanothread (NDNT) enhances interfacial interactions due to its unique surface properties, which improve adhesion with the asphalt matrix. The surface chemistry of DNTs, NDNTs, and CNTs is fundamentally different, leading to variations in interfacial adhesion. Enhanced interfacial adhesion is vital for preventing debonding and ensuring effective stress transfer throughout the modified material. The complexity of asphalt molecules has hindered a thorough understanding of how DNTs, NDNTs, and CNTs reinforce the interfacial properties of asphalt nanocomposites. While previous studies have primarily concentrated on the individual effects of CNTs on asphalt properties, our research uniquely explores the interfacial load transfer capabilities and shear resistance of DNT- and CNT-modified asphalt for the first time. To the best of the authors' knowledge, few studies have clarified the reinforcing mechanisms of DNTs, NDNTs, and CNTs within the asphalt matrix at the atomistic level. The unveiled mechanisms are crucial for understanding the unique interactions between the reinforcements and asphalt, which can aid in predicting and optimizing the performance of DNT-modified asphalt nanocomposites.

1.3 Research motivation

Experimentally investigating DNT-/CNT-reinforced asphalt at the nanoscale is difficult due to the challenges in manipulating and observing nanoscale interactions in the laboratory. Molecular dynamics (MD) simulations provide a powerful and advantageous alternative.[19,20] MD simulations are widely employed to investigate the interfacial behaviors and mechanical properties of DNT-/CNT-modified materials due to the atomistic resolution and ability to capture molecular interactions.

MD simulations have been utilized to study the interfacial contact behaviors between CNTs and asphalt binders, revealing that the addition of multi-walled CNTs can significantly enhance the adhesion ability of asphalt on aggregate surfaces, particularly for alkaline aggregates.[21] The effects of DNT on the glass transition temperature of poly(methyl methacrylate) (PMMA) composites were investigated by MD simulations, demonstrating the exceptionally high glass transition temperatures and low densities of DNT-modified PMMA composites.[22]

Additionally, MD simulations and DFT calculations have been combined to explore the frictional performance of DNT-modified polymer composites, underscoring that DNTs significantly enhance the frictional resistance of polymer composites by the improved interfacial interactions.[23] Furthermore, MD simulation overcomes experimental limitations by enabling the direct visualization and quantification of interactions at the atomistic level, providing atomistic insight into the reinforcement mechanisms between asphalt and DNTs/CNTs.[24–31] Although asphalt consists of complex and diverse components, MD simulation can effectively manage this complexity and offers insights into the interactions between DNTs/CNTs and asphalt molecules.[32,33]

Asphalt properties, including aging, fatigue cracking, and moisture resistance, have been investigated in detail by MD simulations, and the availability and validity of MD can be demonstrated.[6,34,35] Additionally, MD simulations have demonstrated the ability to assess the mechanical strength, thermal conductivity, and interfacial adhesion of DNT/CNT nanomaterials.[36,37] Compared to the high costs and time investments associated with nanoscale experiments, MD offers a more cost-effective and efficient approach to explore a broader range of parameters and predict the performance of DNT-modified asphalt, thus accelerating the development of optimized asphalt nanocomposites.

1.4 Research objective

The objective of this study is to investigate the shear resistance of DNT-/CNT-modified asphalt nanocomposites, comparing

Open Access Article. Published on 28 October 2025. Downloaded on 5/1/2026 11:16:17 PM. This article is licensed under a Creative Commons Attribution-NonCommercial 3.0 Unported Licence.

the initial reinforcing mechanisms between DNTs and CNTs in asphalt nanocomposites. Pullout tests were employed to assess the interfacial load transfer capabilities between asphalt and DNTs/CNTs, while DFT calculations were applied to examine the interfacial binding and electrostatic properties. The results show that the uneven hydrogenated surface of DNTs creates geometric restrictions with the asphalt matrix, facilitating the mechanical interlocking and reducing the mobility of asphalt along the longitudinal direction of DNTs, thereby enhancing load transfer. Hydrogen bonding increases the shear resistance of NDNTs by constraining the molecular motion of asphalt molecules within the matrix.

The binding energy between NDNTs and asphalt molecules is higher than that of other DNTs due to the polarized nitrogen-doping surface. In contrast, CNT-modified asphalt nanocomposites exhibit higher resistance to shear deformation and increased rigidity as compared to DNTs. The π–π stacking interactions are crucial, allowing asphalt molecules to wrap around CNT surfaces, which improves adhesion and load transfer. The delocalized π-electrons of CNTs enhance adhesion to aromatic rings in asphalt. By assessing the effectiveness of DNTs and CNTs in asphalt nanocomposites, we have uncovered new strategies for developing more efficient nanomaterials for asphalt reinforcement, which can significantly enhance the durability and lifespan of asphalt pavement.

2 Model and methodology

2.1 Atomistic model

The 12-molecule model representing AAA-1 asphalt from the Strategic Highway Research Program (SHRP) asphalt systems is employed in this study, and it has been widely adopted in asphalt research.[38] Four components, including asphaltene, polar aromatics, naphthene aromatics, and saturates, are identified in this model, as shown in Fig. 1(a). Each component consists of several representative molecules, which are determined by Hansen solubility parameters and mass fractions of the corresponding elements and components in asphalt.[39] Three molecular structures, namely asphaltene-phenol, asphaltene-pyrrole, and asphaltene-thiophene, were chosen to represent asphaltene molecules, because they more accurately reflect the true asphaltenes and mitigate the 'pentane effect'.[40] The polar aromatics are represented by five different molecules from sedimentary rock samples of geochemistry literature, including quinolinohopane, thioisorenieratane, benzobisbenzothiophene, pyridinohopane, and trimethylbenzeneoxane.[41]

Two naphthene aromatic molecules are identified in this model as perhydrophenanthrene-naphthalene (PHPN) and dioctyl-cyclohexane-naphthalene (DOCHN), possessing the average distribution of aromatic, naphthenic, and paraffinic carbons of crude oils. Finally, hopane and squalene were selected as the saturate components of asphalt, aligning with the direct separation and quantitative analysis of *n*- and iso-alkanes in neat SHRP asphalts. Hopane is typically found in crude oils, while squalene is derived from plant and animal sources and is also present in petroleum.[42] The molecular formula and fractions of different asphalt components are presented in Table 1. The mass ratios of four components in the asphalt model were calculated and are shown in Fig. 2, and are in good accordance with the asphalt from the experimental measurement.[39] The molecular mass ratios assist in determining the balance between the reinforcing capabilities of the nanomaterials and the viscosity of the asphalt, which is essential for ensuring optimal dispersion and interaction within the nanocomposite.

The number of each type of molecule used in our model asphalts was carefully adjusted to align with the experimental data on asphalt speciation and atomic composition from SHRP asphalts.[39] This approach ensures that our model accurately represents the complex composition of real-world asphalt, which typically contains a balance of various sizes and atom types, including carbon, hydrogen, nitrogen, sulfur, and oxygen.[43] Using first-principles calculations, various stable DNT topologies have been found that can be synthesized and characterized using experimental methods.[44]

Three typical DNTs with the same aspect ratios were selected and identified as DNT1, DNT2, and DNT3 in this study, as shown in Fig. 1(b)–(e). These DNTs exhibit sp^3 hybridization and are present at their lowest energy states. DNT1 is derived from a hydrogenated carbon nanotube with a chirality of (3, 0), known for its stability and favorable electronic properties. DNT2 features a coiled structure, providing insights into how curvature affects mechanical properties and interactions with surrounding materials. DNT3 adopts a zigzag configuration, allowing us to explore the effects of this topology on the overall performance and compatibility with asphalt.

Each of these structures exhibits sp^3 hybridization and is present at its lowest energy state, and therefore, they are suitable candidates for our investigations. Additionally, it was proposed to use NDNTs to investigate the influence of heteroatoms on DNTs interacting with asphalt. NDNTs are constructed by substituting the carbon atoms on certain locations of the nanothread backbone with nitrogen atoms, and the nitrogen ratio of the NDNT model is 16.7% to ensure adequate dopants.[45] Furthermore, a molecular structure of CNTs with a chirality of (3, 0) was also constructed to compare to the DNT and NDNT structures with the same aspect ratio. The same length and aspect ratios of DNTs, NDNTs, and CNTs were chosen to ensure a fair comparison in the pullout test.

2.2 Forcefield

In this study, we applied a consistent valence forcefield (CVFF) for the MD simulations due to its broad applicability and proven effectiveness in accurately modeling molecular interactions in asphalt and CNT-based nanomaterials. Although CVFF might possess limitations in modeling highly specific hydrogen bonding or other nuanced interactions compared to COMPASS or PCFF forcefields, it is capable of reliably calculat-

 This journal is © The Royal Society of Chemistry 2025

Open Access Article. Published on 28 October 2025. Downloaded on 5/1/2026 11:16:17 PM.
This article is licensed under a Creative Commons Attribution-NonCommercial 3.0 Unported Licence.

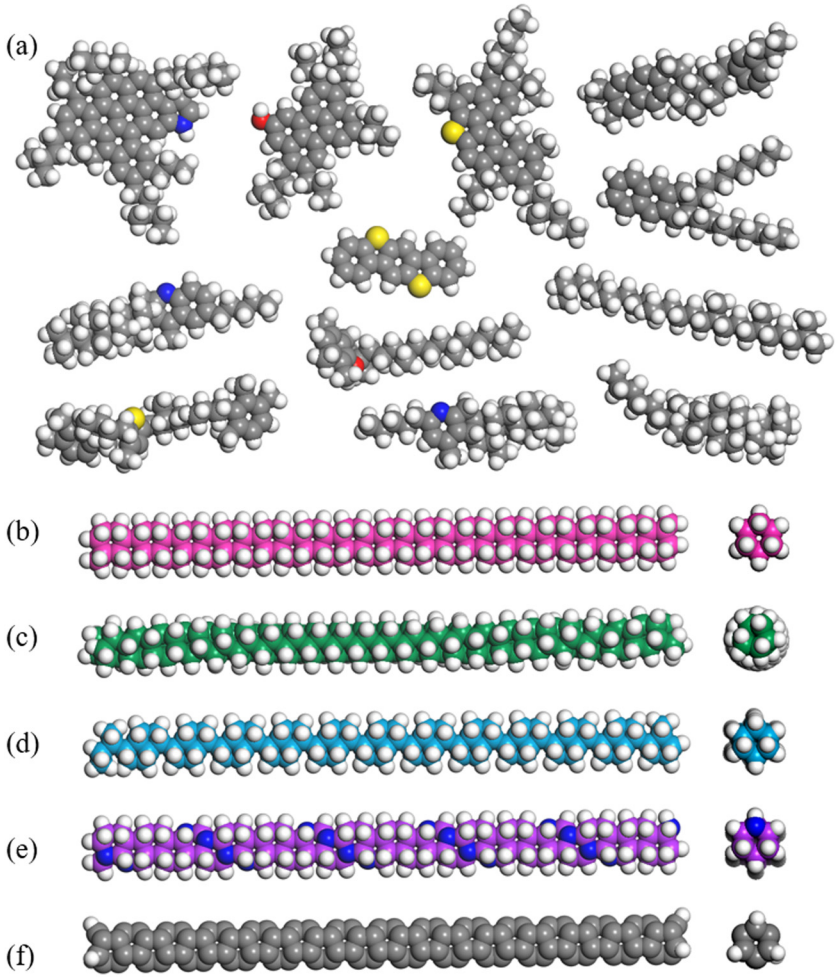

Fig. 1 Atomistic configurations of the (a) 12-molecule asphalt model. Front views and side views of (b) DNT1, (c) DNT2, (d) DNT3, (e) NDNT, and (f) CNT with chirality of (3, 0). (The dark blue atoms on NDNT are doped nitrogen atoms).

Table 1 Molecular formulas and ratios of asphalt components

Component	Molecular type	Molecular formula	Number	Molecular mass (g mol^{-1})	Mass ratio (%)
Asphaltene	Asphaltene-phenol	$C_{42}H_{54}O$	12	574.9	5.3
	Asphaltene-pyrrole	$C_{66}H_{81}N$	8	888.4	5.5
	Asphaltene-thiophene	$C_{51}H_{62}S$	12	707.1	6.5
Polar aromatics	Quinolinohopane	$C_{40}H_{59}N$	16	553.9	6.8
	Thioisorenieratane	$C_{40}H_{60}S$	16	573.0	7.0
	Benzobisbenzothiophene	$C_{18}H_{10}S_2$	60	290.4	13.4
	Pyridinohopane	$C_{36}H_{57}N$	16	503.9	6.2
	Trimethylbenzeneoxane	$C_{29}H_{50}O$	20	414.7	6.4
Naphthene aromatics	PHPN	$C_{35}H_{44}$	44	464.7	15.7
	DOCHN	$C_{30}H_{46}$	52	406.7	16.2
Saturate	Hopane	$C_{30}H_{62}$	16	482.9	5.9
	Squalane	$C_{35}H_{62}$	16	422.8	5.2

ing the essential physical and mechanical properties of asphalt, including density, cohesive energy density, and diffusion coefficient, which are crucial for understanding the behavior of asphalt in various applications.[46,47] Furthermore, CVFF has been successfully employed to investigate the mechanical properties of CNTs and DNTs, capturing their unique bonding characteristics and structural behaviors.[48,49] Additionally, CVFF is well-suited for MD simulations because it effectively treats bonded and non-bonded interactions, ensuring that our simulations accurately reflect the dynamic behaviors of nanocomposites.[50] The functional expression of CVFF is presented as:

Open Access Article. Published on 28 October 2025. Downloaded on 5/1/2026 11:16:17 PM.
This article is licensed under a Creative Commons Attribution-NonCommercial 3.0 Unported Licence.

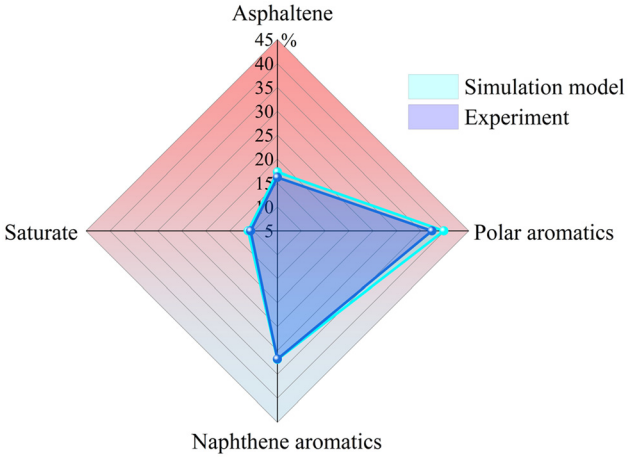

Fig. 2 Differences in mass ratios of four asphalt components between model and experiment.

$$E_{\text{total}} = \sum_{b} K_b(b - b_0)^2 + \sum_{\theta} K_\theta(\theta - \theta_0)^2 + \sum_{\phi} K_\phi[1 + s\cos(n\varphi)] + \sum_{\chi} K_\chi[1 - \cos(2\chi)] + \sum_{\text{nonbond}} \left\{ \varepsilon_{ij}\left[\left(\frac{r_{ij}^o}{r_{ij}}\right)^{12} - \left(\frac{r_{ij}^o}{r_{ij}}\right)^{6}\right] + \frac{q_i q_j}{\varepsilon_0 r_{ij}} \right\} \quad (1)$$

The energy terms are composed of bonded interaction terms and non-bond interaction terms. The bonded interaction terms involve bond interactions, bond angle interactions, torsional angle interactions, and out-of-plane angle interactions. The non-bond interaction terms involve van der Waals interactions and electrostatic interactions. The van der Waals interactions are represented by the LJ-12-6 function, while the electrostatic interactions are described by the coulombic function.

2.3 Simulation method

The adopted asphalt model and forcefield were validated by computing key properties, including density, viscosity, and glass transition temperature (T_g). The density values were obtained from the simulation results after a 1 ns NPT simulation at 300 K and 101 kPa, once the asphalt system reached full equilibrium. The Green–Kubo method[51] is precise and effective for determining the shear viscosity of the asphalt system, and the formula is shown below:

$$\eta = \frac{V}{\kappa_B T}\int_0^\infty \left\langle P_{\alpha\beta}^S(0) P_{\alpha\beta}^S(t)\right\rangle \mathrm{d}t \quad (2)$$

where η refers to the viscosity of asphalt, κ_B refers to the Boltzmann constant, and V and T denote the volume and temperature of the system, respectively. $P_{\alpha\beta}^S(0)$ and $P_{\alpha\beta}^S(t)$ are the instantaneous values of the off-diagonal stress tensor components αβ at the initial time and at a specific time of t, respectively. The glass transition temperature represents the motion characteristics of polymeric materials, specifically referring to the mobility of molecular chains.[52] The glass transition temperature of the asphalt system was determined using a stepwise cooling approach within molecular dynamics simulations. Initially, the system was equilibrated at 420 K for 1 ns under NPT conditions (1 fs timestep, Nose–Hoover thermostat/barostat). The temperature was then lowered in 20 K decrements to 100 K. Each cooling step involved a 150 ps NPT simulation, comprising a 50 ps cooling phase and a 100 ps equilibration period. The specific volume values at each temperature were averaged and recorded. Three independent simulations were performed to ensure statistical accuracy.

The pullout test was conducted to investigate the shear resistance and interfacial interactions between asphalt and DNTs, as depicted in Fig. 3. Before the pullout process, the DNT and CNT structures underwent a thorough equilibration procedure, including initial optimization using a 500 ps NPT ensemble at 300 K and 101 kPa, followed by the application of nonperiodic boundary conditions along the length direction with a 120 Å vacuum gap. A further 200 ps NVT ensemble at 300 K was applied for additional relaxation, simulating realistic conditions during the interaction of DNTs/CNTs with asphalt.

The dragged end of the reinforcement is considered rigid, while the remaining atoms are flexible. The pullout simulation was conducted by applying a constant velocity of 5×10^{-4} Å fs^{-1} to one end of the reinforcement within an NVT ensemble, while the lateral edges of the 10 Å-thick asphalt remained fixed. The pullout velocity was chosen based on the previous pullout speed of CNTs from the asphalt matrix, which can lead to reasonable results.[53] The pullout simulation results were averaged across multiple independent configurations to minimize the random error.

The binding energy and molecular electrostatic potential were computed to investigate the interaction difference between asphalt components and reinforcements. The molecular electrostatic potentials between asphalt and reinforcements were accurately computed using density functional theory (DFT). For these calculations, the generalized gradient-corrected functionals of Perdew–Burke–Ernzerhof (PBE) were applied to assess the electronic properties. The atomic orbital basis set was defined using double numerical plus d-functions, with a global orbital cutoff radius set at 3.3 Å. Geometry optimization and DFT calculations were performed using the DMol3 module in Materials Studio, with an energy convergence tolerance of 0.001 Ha, a maximal force of 0.02 Ha Å^{-1}, and a maximal displacement of 0.001 Å. Incorporating dispersion corrections would increase the complexity and computation time of our DFT calculations; therefore, they were not included to maintain computational efficiency.[54] Additionally, because asphalt and reinforcement materials primarily rely on polar and electrostatic interactions rather than dispersion forces, the necessity for dispersion corrections is less critical.[55] The formula of binding energy (E_{Bind}) is presented as:

$$E_{\text{Bind}} = E_{\text{Asphalt–reinforcement}} - E_{\text{Asphalt}} - E_{\text{Reinforcement}} \quad (3)$$

where $E_{\text{Asphalt–reinforcement}}$ refers to the total energy of the asphalt and reinforcement system, and E_{Asphalt} and

This journal is © The Royal Society of Chemistry 2025

Open Access Article. Published on 28 October 2025. Downloaded on 5/1/2026 11:16:17 PM.
This article is licensed under a Creative Commons Attribution-NonCommercial 3.0 Unported Licence.

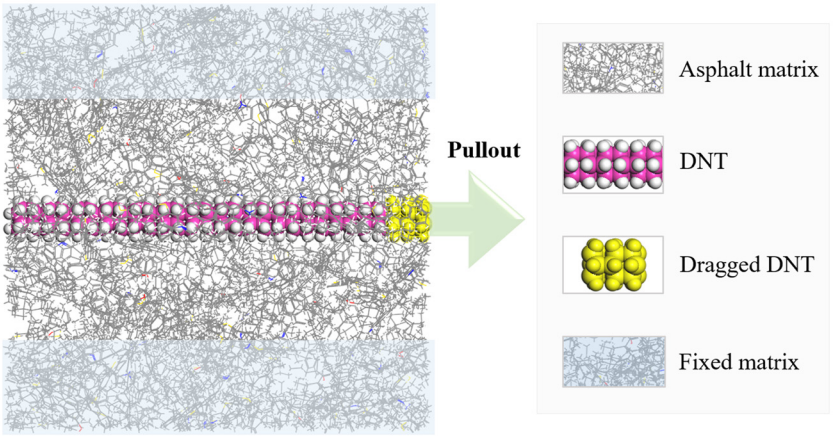

Fig. 3 Diagram of DNT pulled out from the asphalt matrix.

$E_{Reinforcement}$ refer to the energy of the isolated asphalt and the isolated reinforcement, respectively.

The scheme of atomistic modeling and methodology is shown in Fig. 4.

3 Results and discussion

3.1 Model validation

The calculated density values of DNT1, DNT2, DNT3, NDNT, and CNT-modified asphalt nanocomposites are all 1.01 g cm^{-3} (Fig. 5). The density value of pure asphalt is 1.02 g cm^3, showing a 2% deviation from the experimental value of approximately 1.0 g cm^{-3}.[39,56] The density values of DNT-/CNT-modified asphalt nanocomposites are slightly lower than that of pure asphalt, indicating the lightweight feature of DNT-/CNT-modified nanocomposites. The viscosity values of pure asphalt, DNT1-modified asphalt nanocomposite, DNT2-modified asphalt nanocomposite, DNT3-modified asphalt nanocomposite, NDNT-modified asphalt nanocomposite, and CNT-modified asphalt nanocomposite are 1.46 cP, 1.79 cP, 1.72 cP, 1.53 cP, 2.09 cP, and 2.15 cP, respectively. The calculated viscosity is 1.46 cP, which deviates by approximately 3% from the viscosity result of 1.5 cP for the AAA-1 asphalt system.[57]

It was found that DNT/CNT reinforcements can significantly increase the viscosity of asphalt, which was attributed to the increased interactions between DNTs/CNTs and the asphalt matrix. The calculated T_g values of pure asphalt, DNT1-modified asphalt nanocomposite, DNT2-modified asphalt nanocomposite, DNT3-modified asphalt nanocomposite, NDNT-modified asphalt nanocomposite, and CNT-

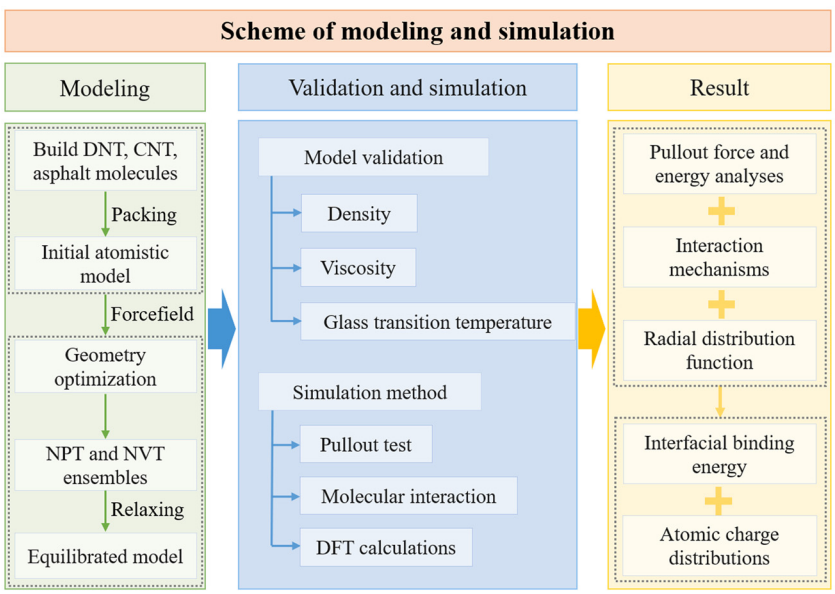

Fig. 4 Schematic diagram of atomistic modeling and simulation.

Open Access Article. Published on 28 October 2025. Downloaded on 5/1/2026 11:16:17 PM.
This article is licensed under a Creative Commons Attribution-NonCommercial 3.0 Unported Licence.

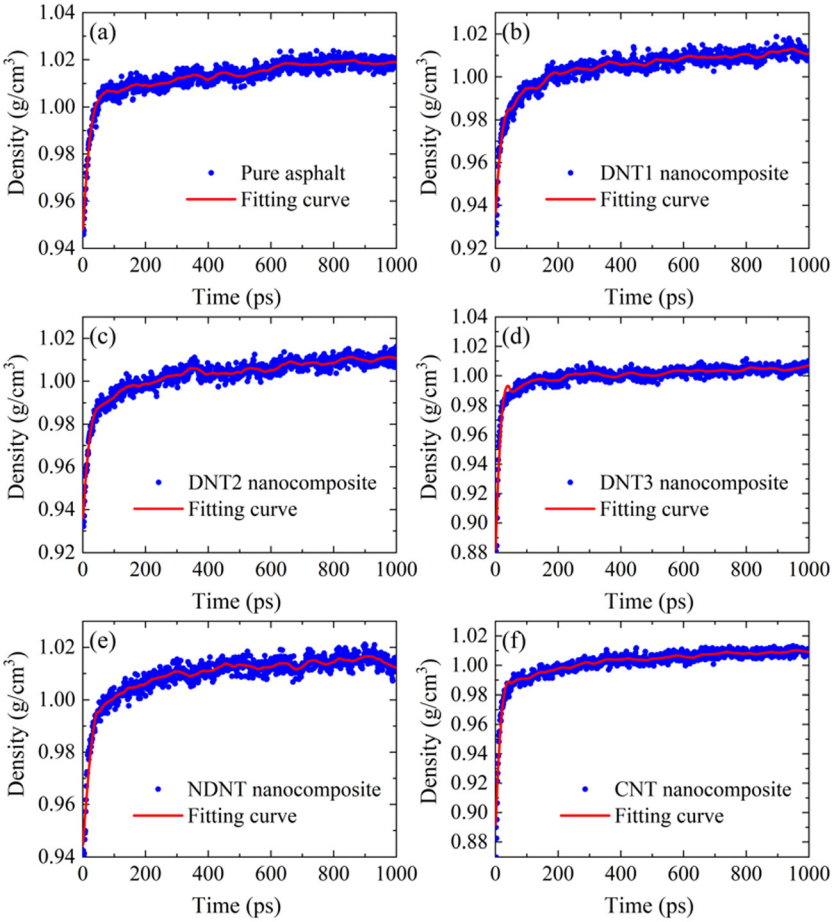

Fig. 5 Density values of (a) pure asphalt, (b) DNT1-modified asphalt nanocomposite, (c) DNT2-modified asphalt nanocomposite, (d) DNT3-modified asphalt nanocomposite, (e) NDNT-modified asphalt nanocomposite, and (f) CNT-modified asphalt nanocomposite during the equilibrium process.

modified asphalt nanocomposite are 246 K, 254 K, 251 K, 260 K, 275 K, and 255 K, respectively. The calculated T_g value is 246 K, with a deviation of approximately 1% from the experimental T_g of 248.56 K for the AAA-1 asphalt system-.[52]

Compared to pure asphalt, the improved T_g values of DNT-/CNT-modified asphalt nanocomposites indicate the enhanced thermal stability and increased deformation resistance to temperature fluctuations. Notably, the NDNT-modified asphalt nanocomposite exhibited a higher viscosity and T_g values than the other DNTs. It is reckoned that nitrogen dopants of DNT structures play a positive role in the overall network strength and stability of DNT-modified asphalt nanocomposites (Fig. 6).

3.2 Pullout test

The pullout tests were carried out to investigate the load-transferring capability between DNTs/CNTs and the asphalt matrix. The snapshots of DNT2, NDNT, and CNT pulled out from asphalt matrixes are depicted in Fig. 7(a)–(c). The deformation continuously occurs perpendicular to the axial direction of the DNTs/CNTs during the pullout process, while no noticeable deformation was observed along the axial direction. Because all DNT/CNT structures with this aspect ratio exhibited high axial stiffness and significantly lower lateral stiffness, they were effective at transferring loads in the axial direction while being laterally weaker. During the pullout process, no asphalt molecules were extracted by the DNTs, although a few asphalt chains bridged the interface between the NDNTs and asphalt. In contrast, there is significantly more interaction between asphalt and CNTs. Several asphalt molecules adhere to the CNT surfaces before complete pullout, and some are transported away once the CNT is fully extracted. These close interactions highlight the strong interfacial bonds and load-transfer capabilities between asphalt and CNTs.

To quantitatively investigate the influence of different topological structures on the reinforcing capability, the force values of the DNT/CNT during the pullout process were calculated and are depicted in Fig. 8. The pullout displacement of the DNT/CNT was recorded within 60 Å, because the DNT/CNT was completely pulled out beyond 60 Å. The pullout force of DNT/CNT rapidly increased at the initial stage, and then fluctuated around a constant value. The root mean square (RMS)

 This journal is © The Royal Society of Chemistry 2025

Open Access Article. Published on 28 October 2025. Downloaded on 5/1/2026 11:16:17 PM.
This article is licensed under a Creative Commons Attribution-NonCommercial 3.0 Unported Licence.

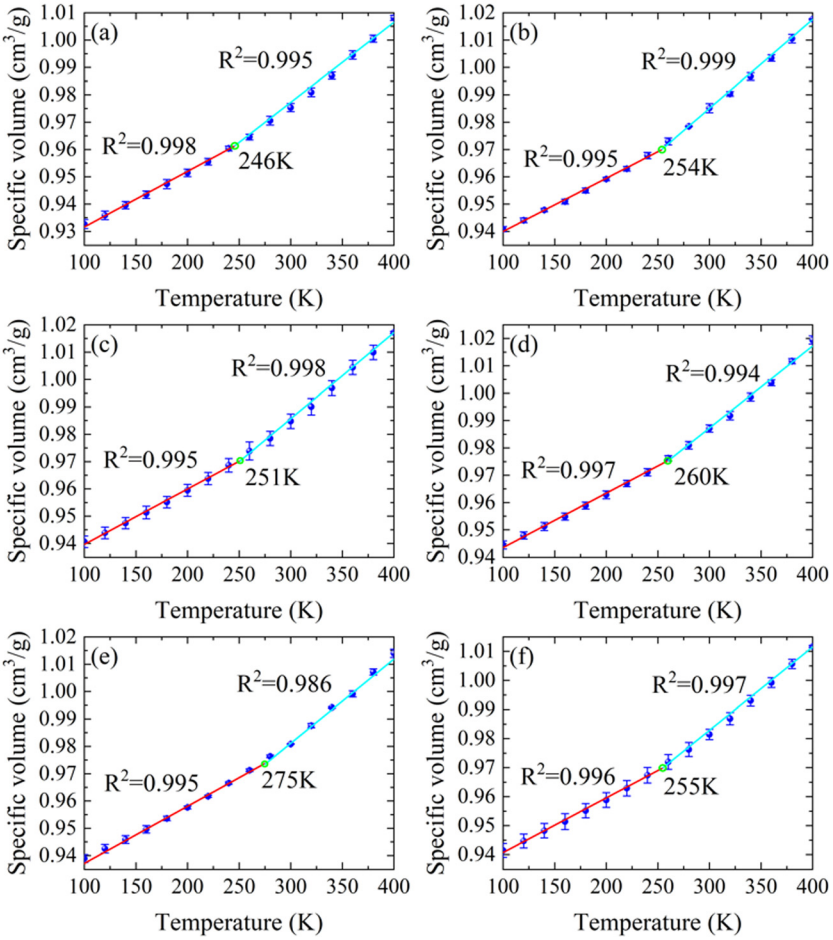

Fig. 6 The specific volume values of (a) pure asphalt, (b) DNT1-modified asphalt nanocomposite, (c) DNT2-modified asphalt nanocomposite, (d) DNT3-modified asphalt nanocomposite, (e) NDNT-modified asphalt nanocomposite, and (f) CNT-modified asphalt nanocomposite at different temperatures. The T_g values of DNT-/CNT-modified asphalt nanocomposites are relatively higher than those of pure asphalt, indicating the higher deformation resistance to temperature changes.

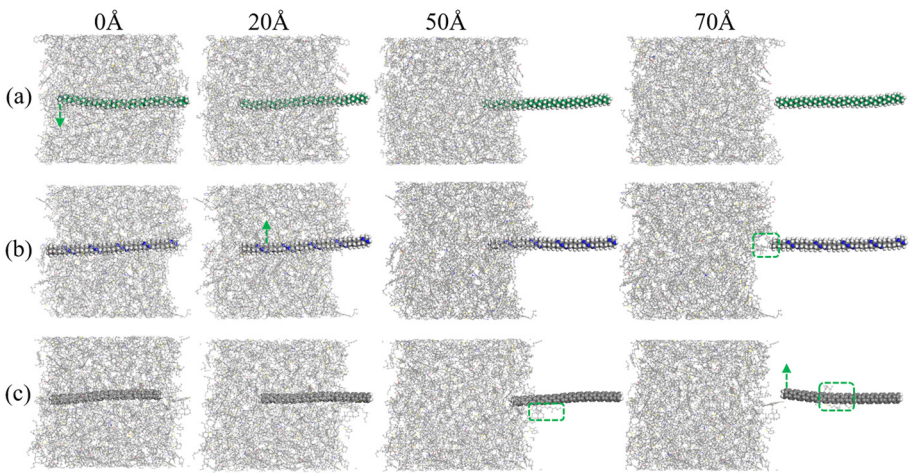

Fig. 7 Snapshots of (a) DNT2, (b) NDNT, and (c) CNT pulled out from the asphalt matrix.

Open Access Article. Published on 28 October 2025. Downloaded on 5/1/2026 11:16:17 PM.
This article is licensed under a Creative Commons Attribution-NonCommercial 3.0 Unported Licence.

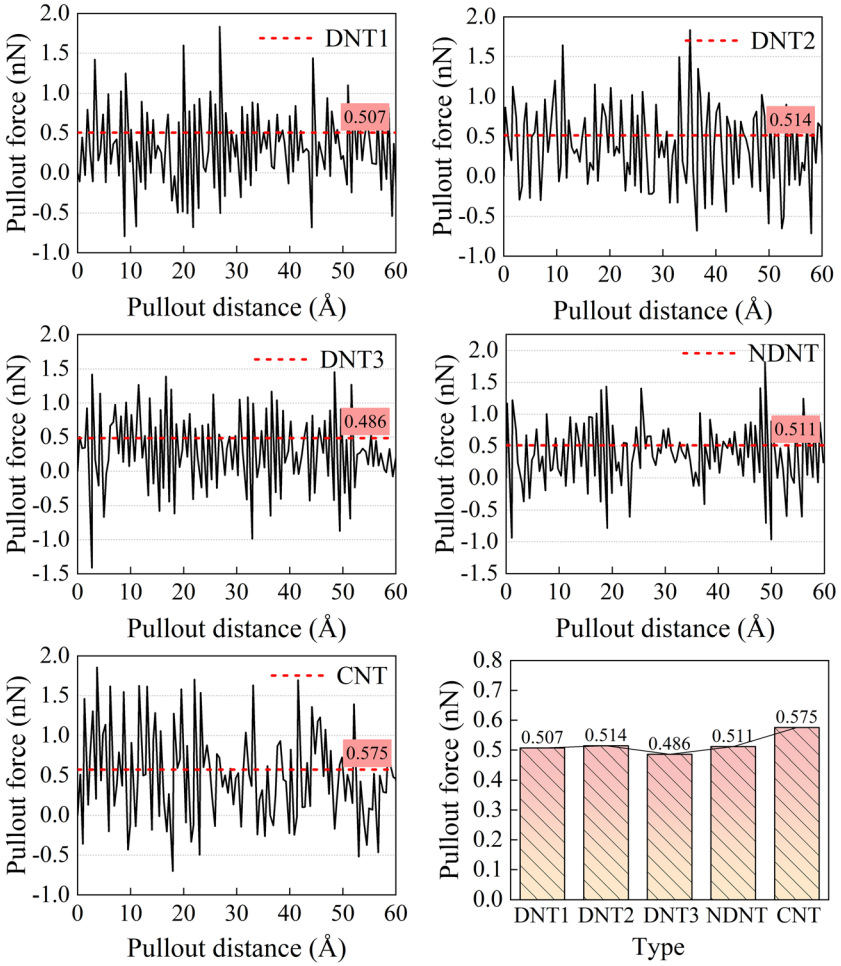

Fig. 8 Pullout force changes with respect to the pullout distance during the pullout process. (The red line indicates the RMS value of the dataset).

values of pullout force were extracted to quantitatively assess the pullout performance of the DNT/CNT. The RMS values of pullout force for DNT1, DNT2, DNT3, NDNT, and CNT are 0.507 nN, 0.514 nN, 0.486 nN, 0.511 nN, and 0.575 nN, respectively. This demonstrates that the CNT-modified asphalt nanocomposite possessed the highest pullout force among all the nanotubes, which echoes the findings that CNTs initiate stronger interfacial interactions.

The pullout force of the DNT2-modified asphalt nanocomposite was the highest among the DNTs. The improved pullout performance of DNT2 was attributed to its helical structure, which enhanced mechanical interlocking within the asphalt matrix and minimized relative movement between the asphalt and DNT2. The pullout force of the NDNT was comparable to that of DNT2, whereas DNT3 exhibited the lowest pullout force among all the DNT variants. Additionally, the NDNT gave a significantly higher pullout performance than that of DNT1, suggesting that the nitrogen-doping of atoms can enhance the interfacial interactions between the asphalt and the nanotubes.

The pullout energy curves of the DNT, NDNT, and CNT during the pullout process are presented in Fig. 9. The pullout

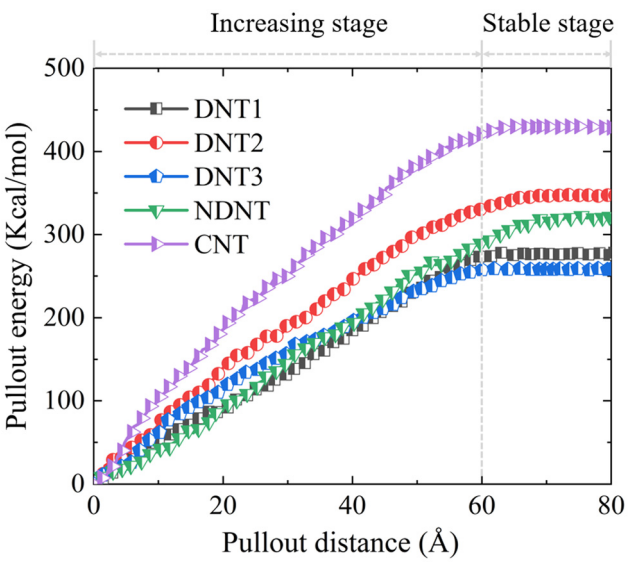

Fig. 9 Pullout energy fluctuations with displacement during the pullout process.

This journal is © The Royal Society of Chemistry 2025

Open Access Article. Published on 28 October 2025. Downloaded on 5/1/2026 11:16:17 PM.
This article is licensed under a Creative Commons Attribution-NonCommercial 3.0 Unported Licence.

energy of the DNT/CNT steadily increased up to 60 Å, ultimately reaching its peak value, which refers to the complete extraction from the asphalt matrix. The pullout energy of the CNT was the highest, at approximately 1.5 times greater than that of DNT2 and DNT3. The increased pullout energy revealed that the CNT-modified asphalt nanocomposite exhibited greater resistance to shear deformation, contributing to its overall rigidity. The pullout energy of DNT2 was the highest among the DNT reinforcements, which was in accordance with its significantly greater pullout force, as discussed in the previous section.

The pullout energy of the NDNT was slightly lower than that of DNT2, but still surpassed that of DNT1 and DNT3. DNT3, with its zigzag structure, exhibited the lowest pullout energy and load-transfer capacity within the asphalt matrix. Notably, the pullout energy of DNT3 was higher than that of DNT1 up to 47 Å, but fell below that of DNT1 beyond this distance. As demonstrated in Fig. 8, the pullout force of DNT3 decreased more rapidly when the pullout distance exceeded 47 Å, resulting in the lower pullout energy.

The molecular interaction details at DNT and asphalt interfaces are demonstrated in Fig. 10(a). The hydrogen atoms on the hydrogenated DNT surface can mechanically interlock with the asphalt atoms at the interface, which contributed to the shear resistance during the pullout process. A schematic representation of the interlocking effect between DNTs and asphalt is depicted in Fig. 10(b). The uneven hydrogenated surface of DNTs creates geometric constraints within the asphalt matrix, facilitating the mechanical interlocking interactions. This interaction reduced the mobility of asphalt along the longitudinal direction of the reinforcement, thereby enhancing mechanical interlocking and improving the load transfer capabilities between the DNT and the asphalt matrix.

The H-bond interaction between the NDNT and asphaltene is presented in Fig. 10(c). It shows that the hydroxyl group on asphaltene-phenol can interact with the nitrogen atoms on NDNTs to generate the O–H···N H-bond. The H-bond interaction contributes to the enhanced shear resistance of NDNTs by increasing the motion constraints within the asphalt matrix, in contrast to DNTs without the nitrogen dopant. The π–π stacking interactions between CNTs and the naphthene aromatic molecule (DOCHN) are presented in Fig. 10(d).

The π–π stacking interactions are crucial for enhancing the shear resistance of asphalt, facilitating the wrapping of asphalt molecules around the surface of CNTs. It was found that the ratios of aromatic carbon can constitute up to 40% of the total carbon content of asphalt, and were primarily derived from components including asphaltenes, polar aromatics, and naphthene aromatics.[39] These molecules can generate a significant number of π–π stacking interactions around CNTs,

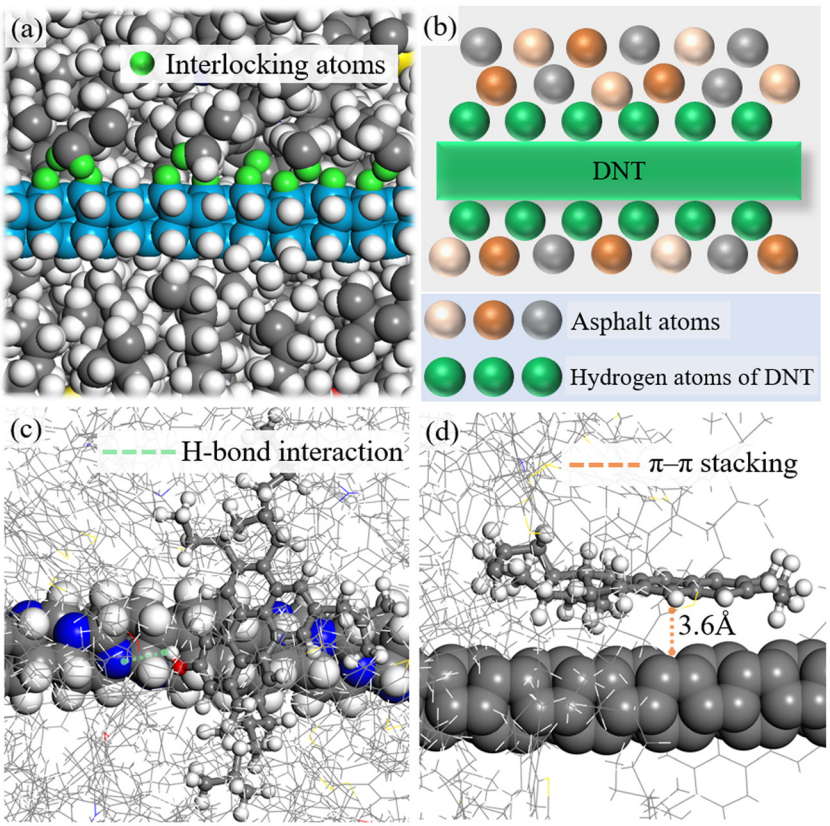

Fig. 10 Molecular details at the (a) DNT and asphalt interface. (b) A schematic illustration of the interlocking effect at the DNT-asphalt interface. (c) H-bond interaction between NDNT and an asphaltene molecule. (d) π–π stacking interaction between CNT and a naphthene aromatic molecule.

Open Access Article. Published on 28 October 2025. Downloaded on 5/1/2026 11:16:17 PM.
This article is licensed under a Creative Commons Attribution-NonCommercial 3.0 Unported Licence.

thereby enhancing the overall load transfer capabilities of CNTs during the deformation and pullout process.

The radial distribution function (RDF) curves between DNTs/CNTs and asphalt components are depicted in Fig. 11(a)–(c). The $g(r)$ values for naphthene aromatics and DNTs peak within 8 Å, indicating stronger interactions between the two. The molecular chains of naphthene aromatic molecules, including DOCHN, can interact with the DNT surface through mechanical interlocking, leading to enhanced interactions. The $g(r)$ curves between NDNTs and asphalt molecules are depicted in Fig. 11(d). The $g(r)$ values between the saturate and NDNTs are higher than those of polar aromatics, asphaltene, and naphthene aromatics. The chain-like structures of saturates can mechanically intertwine with NDNTs and enhance their interactions. Additionally, the nitrogen atoms on NDNTs can engage in hydrogen bonding with the heteroatoms of asphaltenes and polar aromatics, further enhancing these interactions.

As illustrated in Fig. 11(e), the $g(r)$ values between saturates and CNTs are comparatively lower than those for other asphalt components. This suggests that CNTs interact more closely with asphaltenes, polar aromatics, and naphthene aromatics, while exhibiting fewer active interactions with saturate molecules. This discrepancy arises from the enhanced interactions of CNTs with aromatic carbons through π–π stacking, which is a feature absent in saturate molecules. The RDF curves between DNTs/CNTs and asphalt are shown in Fig. 11(f). This demonstrates that DNTs and NDNTs exhibit higher $g(r)$ values than CNTs within 3.6 Å, while showing lower values beyond this threshold. This divergence stems from the distinct surface morphological characteristics between DNTs and CNTs. The hydrogenated surface of DNTs engages more intimately with asphalt molecules through mechanical interlocking, whereas π–π stacking interactions between CNTs and asphalt begin to prevail at approximately 3.6 Å. Notably, the $g(r)$ values between CNTs and asphalt are higher than those for DNTs and NDNTs from 3.6 Å to 16 Å, suggesting stronger interactions between asphalt and CNTs within this distance.

3.3 DFT calculations

Binding energy provides a quantitative measure of the interfacial interactions between asphalt and reinforcements.[58] The

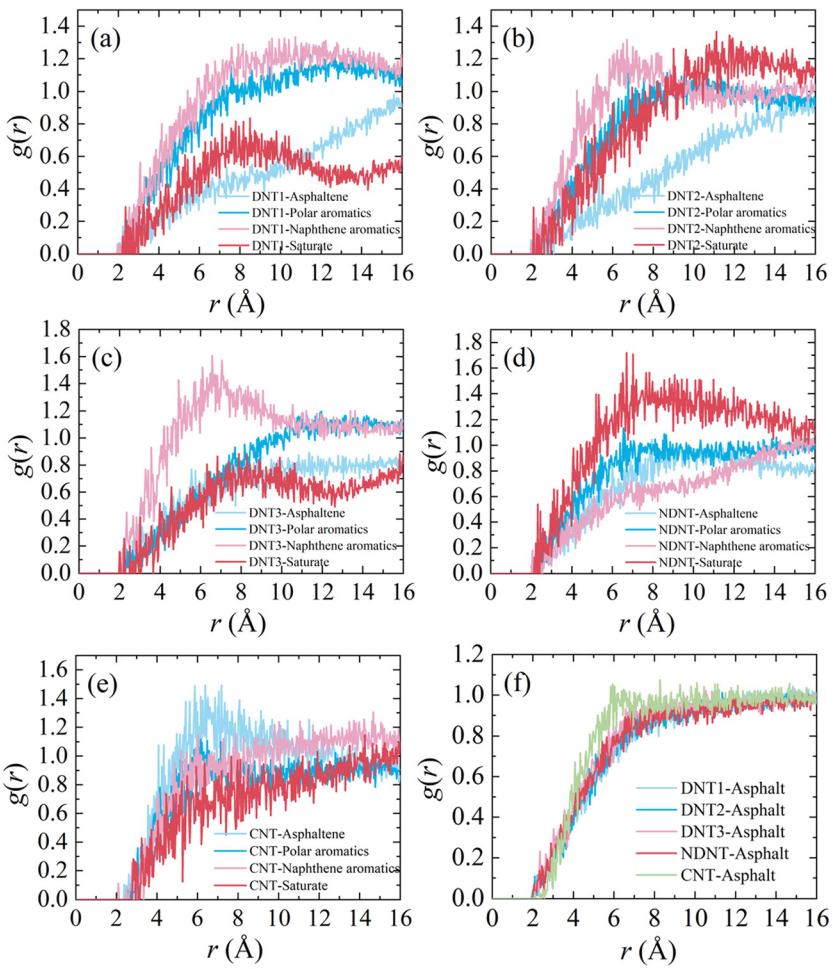

Fig. 11 RDF curves between asphalt components and (a) DNT1, (b) DNT2, (c) DNT3, (d) NDNT, and (e) CNT after full equilibrium. (f) RDF curves between DNTs/CNTs and asphalt molecules after full equilibrium.

This journal is © The Royal Society of Chemistry 2025

Open Access Article. Published on 28 October 2025. Downloaded on 5/1/2026 11:16:17 PM.
This article is licensed under a Creative Commons Attribution-NonCommercial 3.0 Unported Licence.

binding energy values between different asphalt components and DNTs/CNTs are presented in Fig. 12, which shows that the binding energy values between polar components and DNTs/CNTs are relatively higher than those between nonpolar asphalt components and DNTs/CNTs. This indicates that the heteroatoms in the polar components of asphalt are essential for improving interfacial interactions with DNTs/CNTs.

Among all asphalt components, the binding energy between asphaltene and DNTs/CNTs is the highest, primarily due to the larger molecular volume of asphaltene and the presence of heteroatoms. The binding energy values for DNT2 and DNT3 are the lowest among all components, with DNT2 showing an interaction of 13.7 kcal mol^{-1} with saturates, and DNT3 exhibiting 13.8 kcal mol^{-1} with naphthene aromatics. NDNTs achieved the highest binding energy with asphalt components, except for polar aromatics, where their value is slightly lower than that of CNTs. The binding energy between NDNTs and asphaltene is 55.8 kcal mol^{-1}, which is comparatively higher than the 49.9 kcal mol^{-1} observed for CNTs, and much greater than the 40 kcal mol^{-1} for DNT1, 34.5 kcal mol^{-1} for DNT2, and 35.7 kcal mol^{-1} for DNT3. This increased binding energy is attributed to the presence of polarized nitrogen atoms in NDNTs, which enhances the interfacial interactions between NDNTs and asphalt molecules.

The binding energy between CNTs and asphalt is slightly lower than that of NDNTs, but significantly higher than that of DNTs. As previously mentioned, the aromatic rings in asphalt molecules can interact with CNTs and adhere to their surfaces through π–π stacking interactions, thereby enhancing interfacial interactions. Additionally, it has been observed that the binding energy values between DNT1 and asphalt molecules are the highest among the DNTs. DNT2 and DNT3 exhibit significantly lower binding energy compared to others, indicating weaker interactions between asphalt molecules and DNT2/DNT3. The reduced binding energy at the DNT-asphalt interface can be ascribed to the hydrogen passivation of the DNT surface.

The atomic charge distributions between asphalt and DNTs/CNTs are demonstrated through molecular electrostatic potential maps, which can provide detailed insights into the mechanisms underlying interfacial interactions. The molecular electrostatic potentials between DNTs/CNTs and asphalt molecules were calculated and are depicted in Fig. 13. The positive potential is denoted by the red color on the molecules, while the negative potential is represented by the blue color.

As shown in Fig. 13(a)–(c), DNTs exhibit positive potential on the hydrogen atoms and negative potential on the carbon atoms of the backbone, generating a relatively rough electrostatic potential map. Because the rough electrostatic potential of DNTs assists in creating potential energy wells that trap the aliphatic chains of asphalt molecules, it is energetically unfavorable for them to move along the axis of DNTs. The interactions between DNTs and asphalt molecules are mainly governed by a combination of van der Waals forces, electrostatic attractions, and mechanical interlocking.

In contrast to DNTs, the presence of nitrogen dopants can alter the electronic structure of NDNTs, as shown in Fig. 13(d). This leads to the creation of localized negative charges, enhancing the overall electronegativity. The nitrogen atoms of NDNTs exhibit strong negative potentials, while the hydrogen atom connected to the nitrogen atom on asphaltene exhibits strong positive potentials. The interactions between NDNTs

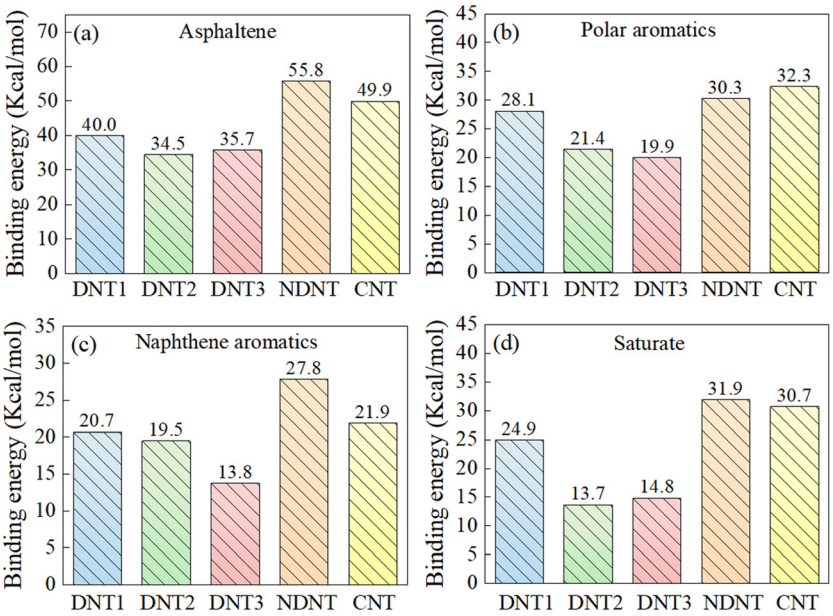

Fig. 12 Binding energy between (a) asphaltene and DNTs/CNTs, (b) polar aromatics and DNTs/CNTs, (c) naphthene aromatics and DNTs/CNTs, and (d) saturate and DNTs/CNTs. The binding energy between NDNTs and asphalt components is relatively higher than that of other DNTs, which was attributed to the polarized nitrogen-doped surface.

Open Access Article. Published on 28 October 2025. Downloaded on 5/1/2026 11:16:17 PM.
This article is licensed under a Creative Commons Attribution-NonCommercial 3.0 Unported Licence.

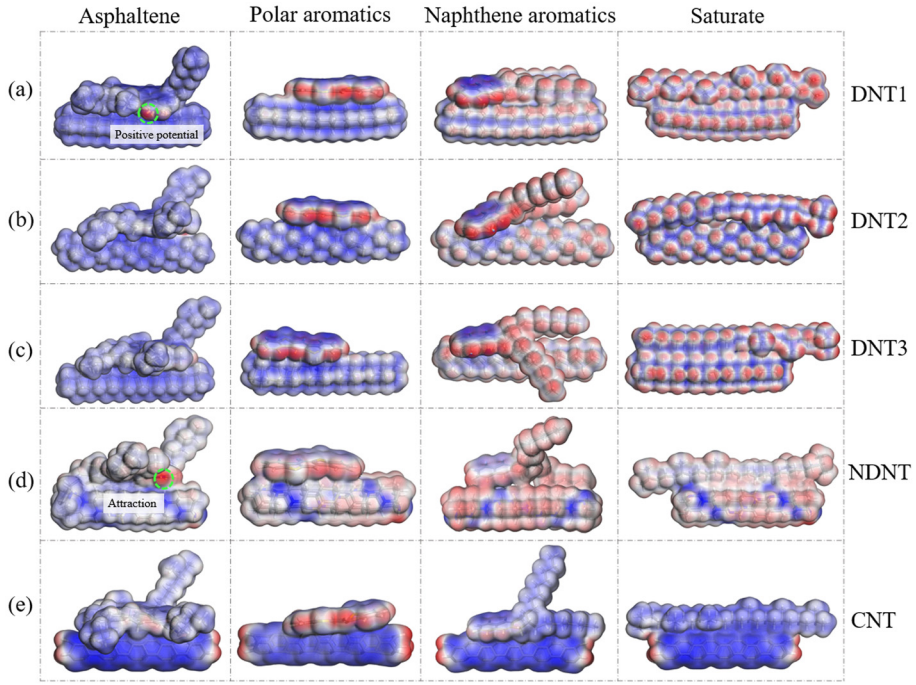

Fig. 13 Molecular electrostatic potentials between asphalt components and (a) DNT1, (b) DNT2, (c) DNT3, (d) NDNTs, and (e) CNTs through DFT calculations.

and asphaltene can be significantly enhanced by the attraction between the electropositive regions of asphaltene and the electronegative domain of NDNTs. The strong electrostatic attraction contributes to the bonding and adhesion between NDNTs and asphaltene, enhancing the overall stability and compatibility.

As presented in Fig. 13(e), there are electronegative domains on the CNT surface, but electropositive domains on the ends of the hydrogen atoms on CNTs. The electrostatic potential on the CNT surface is comparatively smooth, because the delocalized π-electrons in the CNT structure result in a more even distribution of electron density along the surface. The delocalized π-electrons in CNTs can engage in π–π stacking interactions with the aromatic rings in asphalt molecules, leading to stronger adhesion and load transfer capability.

4 Conclusions and discussion

4.1 Conclusions

The shear resistance and interfacial properties of asphalt nanocomposites reinforced with DNTs and CNTs were investigated through MD simulations, focusing on interfacial interactions during the pullout process. The findings revealed that NDNT-modified asphalt nanocomposites exhibit higher viscosity and T_g values compared to other DNTs, while CNT-modified composites demonstrate a greater pullout force as compared to those reinforced with DNTs. This improvement in shear resistance is primarily due to π–π stacking interactions that facilitate the wrapping of asphalt molecules around CNT surfaces. This improvement in shear resistance is crucial for pavement applications, as it enhances the material's ability to withstand mechanical stresses, reducing deformation over time.

Among the DNTs, DNT2-modified asphalt nanocomposites exhibited the highest pullout performance, which was attributed to DNT2's helical structure, which promoted mechanical interlocking and reduced relative movement within the asphalt matrix. Additionally, the hydrogenated surface of DNT enhanced interactions with asphalt molecules, and the formation of O–H···N hydrogen bonds between hydroxyl groups on asphaltene-phenol and nitrogen atoms on NDNTs further increased the shear resistance. Although the binding energy between CNT and asphalt is slightly lower than that of NDNTs, it remains significantly higher than that of DNTs. DFT calculations indicate that nitrogen doping modifies the electronic structure of NDNTs, resulting in localized negative charges that enhance electronegativity, while delocalized π-electrons in CNTs improve adhesion and load transfer capabilities.

These findings suggest that incorporating NDNTs and CNTs into asphalt mixtures can lead to more sustainable and resilient pavement materials with improved long-term durability. Overall, this study underscores the considerable potential of DNTs, NDNTs, and CNTs when developing sustainable and resilient asphalt nanocomposites for the pavement industry. Importantly, our research extends beyond pavement applications, offering broader implications for materials science and nanotechnology. By clarifying the interfacial interactions and mechanisms at play, our work paves the way for further

 This journal is © The Royal Society of Chemistry 2025

Open Access Article. Published on 28 October 2025. Downloaded on 5/1/2026 11:16:17 PM. This article is licensed under a Creative Commons Attribution-NonCommercial 3.0 Unported Licence.

exploration of nanomaterials in various composite systems, promoting interdisciplinary research and collaboration.

By investigating the shear resistance and interfacial properties of asphalt nanocomposites reinforced with DNTs and CNTs through molecular dynamics simulations, we explored fundamental interactions that enhanced the performance of asphalt material. The unique properties of DNTs, such as their helical structure and hydrogenated surfaces, significantly improved mechanical interlocking and interfacial interactions with asphalt, which are critical for developing sustainable and resilient materials. Additionally, our findings on electronic structure modifications due to nitrogen doping in NDNTs further contribute to understanding how nanomaterials can optimize the performance of composite systems.

By examining these differences at the atomistic level, our study not only clarifies the unique roles of DNTs and CNTs, but it also contributes new insights when optimizing asphalt nanocomposites for improved durability and performance. This emphasis on comparative analysis and the exploration of new reinforcement mechanisms represents a significant advancement over prior works, paving the way for more effective applications of nanomaterials and other nanocomposite materials across various applications, including lightweight structural materials, energy storage systems, and advanced coatings. Our work not only addresses immediate challenges in the field of asphalt technology, but it also opens avenues for interdisciplinary research that could benefit a wide range of applications.

4.2 Discussion

While MD simulations are effective for investigating the interfacial interactions of various materials, they inherently operate on a timescale ranging from nanoseconds to microseconds. This limitation restricts the ability to observe the long-term behaviors of asphalt nanocomposites, including aging and fatigue processes. Consequently, although we have revealed improvements of DNTs/CNTs in shear resistance and interfacial properties, these enhancements may not accurately reflect the performance of asphalt materials over extended periods in real-world conditions.

To address these limitations, future research could include complementary approaches, such as experimental studies that monitor the long-term performance of DNT-/CNT-modified asphalt nanocomposites under realistic conditions. Additionally, employing multi-scale modeling techniques that bridge the gap between molecular dynamics and continuum mechanics could provide valuable insights into the macroscopic behavior of these materials over longer time scales.

The effectiveness of nanomaterials in enhancing asphalt properties relies heavily on the interfacial interactions between the nanomaterials and the asphalt matrix. In a homogeneous distribution, each nanomaterial can uniformly interact with asphalt molecules, promoting effective load transfer and increased shear resistance. However, in a heterogeneous arrangement, some regions may experience stronger interactions, while others may not benefit from reinforcement, leading to inconsistent performance. This variability in distribution can arise from factors such as mixing techniques and processing conditions, which may not be fully controlled in practical applications.

In the MD simulations, we assumed a homogeneous distribution of nanomaterials within the asphalt matrix. Consequently, there may be discrepancies between the simulations and experiments with regard to the mechanical properties of the asphalt nanocomposite. Therefore, future studies should explore the effects of different nanomaterial distributions to provide a more comprehensive understanding of their impact on asphalt performance.

Conflicts of interest

There are no conflicts to declare.

Data availability

The raw simulation data, input files for the LAMMPS simulations,[59] and analysis scripts used to generate the findings reported in this study are not publicly deposited in a repository due to their large size and specialized formatting, but they are available from the corresponding author, Dr Xuefeng LIU (xfliu6-c@my.cityu.edu.hk), upon reasonable request. The CVFF forcefield parameters used in this study are derived from previously published and cited works,[60,61] while the LAMMPS software package[62] employed for the simulations is publicly available. Additionally, all other relevant data and methodological details necessary for understanding and reproducing the conclusions of this manuscript are provided within the article.

Acknowledgements

The authors are grateful for the support from the National Natural Science Foundation of China (Grant No. 42277175 and 12102162) and the Guizhou Provincial Major Scientific and Technological Program (2023-425).

References

1 T. Nian, P. Li, J. Ge, J. Song and M. Wang, Green environmental protection and sustainable utilization of straw: Investigation for molecular dynamics of highland barley straw fiber to enhancing road performance of asphalt, *J. Cleaner Prod.*, 2024, **452**, 141940.
2 A. Behnood, A review of the warm mix asphalt (WMA) technologies: Effects on thermo-mechanical and rheological properties, *J. Cleaner Prod.*, 2020, **259**, 120817.
3 X. Luo, J. Xu and F. Ma, Thermodynamics of healing of asphalt binders with free energy, *Mech. Mater.*, 2023, **185**, 104757.

Open Access Article. Published on 28 October 2025. Downloaded on 5/1/2026 11:16:17 PM. This article is licensed under a Creative Commons Attribution-NonCommercial 3.0 Unported Licence.

4 M. S. Bello, Y. Zhang, X. Wang and N. S. A. Yaro, Recycling polymeric healthcare waste in asphalt pavements towards sustainable roads: A technical review, *J. Cleaner Prod.*, 2024, **480**, 144068.
5 Y. Wang, W. Wang and L. Wang, Understanding the relationships between rheology and chemistry of asphalt binders: A review, *Constr. Build. Mater.*, 2022, **329**, 127161.
6 C. Yan, J. Yan, Z. Zhang, D. Yu, S. Wang, X. Jiang, C. Ai and Z. Leng, Screw extrusion process used in the polymer modified asphalt field: A review, *J. Cleaner Prod.*, 2024, **448**, 141592.
7 H. Li, S. Liu, F. Yang, S. He, H. Jing, X. Zou, Z. Li and Y. Sheng, Review of utilization of bamboo fiber in asphalt modification: Insights into preparation, performance, reinforcement, and challenges, *J. Cleaner Prod.*, 2024, **468**, 143010.
8 P. Lin, X. Liu, S. Ren, Y. Li, J. Xu and M. Li, Unraveling the influence of fibers on aging susceptibility and performance of high content polymer modified asphalt mixtures, *Case Stud. Constr. Mater.*, 2023, **18**, e02211.
9 I. R. Segundo, E. Freitas, V. T. F. C. Branco, S. Landi, M. F. Costa and J. O. Carneiro, Review and analysis of advances in functionalized, smart, and multifunctional asphalt mixtures, *Renewable Sustainable Energy Rev.*, 2021, **151**, 111552.
10 J. Zhou, A. I. Chizhik, S. Chu and D. Jin, Single-particle spectroscopy for functional nanomaterials, *Nature*, 2020, **579**, 41–50.
11 K. Debbarma, B. Debnath and P. P. Sarkar, A comprehensive review on the usage of nanomaterials in asphalt mixes, *Constr. Build. Mater.*, 2022, **361**, 129634.
12 D. Mitra, S. Faisal Kabir, A. Ali, Y. Mehta and M. Elshaer, Evaluation of the impact of nanomodification on Self-Healing behavior of asphalt binders, *Constr. Build. Mater.*, 2023, **405**, 133358.
13 D. Zhang, Z. Huang, G. Yuan, Y. Zheng, G. Qian, Z. You and H. Zhang, Research on the anti-aging mechanism of SBS-modified asphalt compounded with multidimensional nanomaterials based on atomic force microscopy, *Constr. Build. Mater.*, 2022, **317**, 125808.
14 Y. Li, L. Yang, X. Jiang, Y. Lu, C. Han, Y. Tang and N. Yang, Diamond Nanostructures at Different Dimensions: Synthesis and Applications, *Adv. Funct. Mater.*, 2024, **34**, 30.
15 H. Zhan, G. Zhang, V. B. Tan and Y. Gu, The best features of diamond nanothread for nanofibre applications, *Nat. Commun.*, 2017, **8**, 14863.
16 H. Zhan, G. Zhang, X. Zhuang, R. Timon and Y. Gu, Low interfacial thermal resistance between crossed ultra-thin carbon nanothreads, *Carbon*, 2020, **165**, 216–224.
17 K. Duan, J. Zhang, L. Li, Y. Hu, W. Zhu and X. Wang, Diamond nanothreads as novel nanofillers for cross-linked epoxy nanocomposites, *Compos. Sci. Technol.*, 2019, **174**, 84–93.
18 X. Q. Wang, C. L. Chow and D. Lau, Topology-controlled thermomechanical properties of diamond nanothread enhanced polymeric materials, *Appl. Mater. Today*, 2023, **32**, 101822.
19 Y. Feng, H. Hao, H. Lu, C. L. Chow and D. Lau, Exploring the development and applications of sustainable natural fiber composites: A review from a nanoscale perspective, *Composites, Part B*, 2024, **276**, 111369.
20 X. Q. Wang, W. Jian, O. Buyukozturk, C. K. Y. Leung and D. Lau, Degradation of epoxy/glass interface in hygrothermal environment: An atomistic investigation, *Composites, Part B*, 2021, **206**, 108534.
21 W. Cui, W. Huang, H. M. Z. Hassan, X. Cai and K. Wu, Study on the interfacial contact behavior of carbon nanotubes and asphalt binders and adhesion energy of modified asphalt on aggregate surface by using molecular dynamics simulation, *Constr. Build. Mater.*, 2022, **316**, 125849.
22 W. M. Ji and L. W. Zhang, Diamond nanothread reinforced polymer composites: Ultra-high glass transition temperature and low density, *Compos. Sci. Technol.*, 2019, **183**, 107789.
23 B. B. Yin, J. S. Huang, W. M. Ji and K. M. Liew, Exploring frictional performance of diamond nanothread reinforced polymer composites from the atomistic simulation and density functional theory, *Carbon*, 2022, **200**, 10–20.
24 X. Liu, R. Yang, Z. Bie, F. Nie, Y. Fan, E. Oterkus and X. He, Enhanced interfacial thermal transport in diamond nanothread reinforced polymer nanocomposites: insights from atomistic simulations and density functional theory, *Nanoscale*, 2025, **17**, 13419–13433.
25 F. Nie, X. Su, M. Wang, X. Ma, K. Ou, J. Liu and H. Lin, Debonding of asphalt-aggregate interface under coupled moisture and temperature conditions: An atomistic study, *Case Stud. Constr. Mater.*, 2025, **22**, e04554.
26 F. Nie, Z. Bie and H. Lin, Investigating the advanced thermomechanical properties of coiled carbon nanotube modified asphalt, *Constr. Build. Mater.*, 2024, **441**, 137512.
27 B. Cui and H. Wang, Molecular modeling of asphalt-aggregate debonding potential under moisture environment and interface defect, *Appl. Surf. Sci.*, 2022, **606**, 154858.
28 X. Ma, X. Zhu, T. Wang, T. Si and J. Fan, Unveiling the importance of surface ionization on desalination and ion-sieving performance of graphene oxide membranes, *Sep. Purif. Technol.*, 2024, **341**, 126930.
29 S. Kumar, Investigating effect of CNT agglomeration in CNT/polymer nanocomposites using multiscale finite element method, *Mech. Mater.*, 2023, **183**, 104706.
30 Q. L. Xiong, S. A. Meguid, Y. Wang and G. J. Weng, Molecular dynamics and atomistic based continuum studies of the interfacial behavior of nanoreinforced epoxy, *Mech. Mater.*, 2015, **85**, 38–46.
31 F. Nie, W. Jian, Z. Yu, C. L. Chow and D. Lau, Mesoscale modeling to study isolated asphaltene agglomerates, *Constr. Build. Mater.*, 2023, **379**, 131249.
32 J. Zhang, L. Sun, H. Zhan, Y. Nie, Y. Pang, C. Bian and C. Lü, Impact of diamond nanothread on the viscosity of

Open Access Article. Published on 28 October 2025. Downloaded on 5/1/2026 11:16:17 PM. This article is licensed under a Creative Commons Attribution-NonCommercial 3.0 Unported Licence.

asphalt binder: Insights from atomistic simulations, *J. Cleaner Prod.*, 2024, **434**, 139945.

33 Z. Luo, J. Guo, X. Liu, Y. Mu, M. Zhang, M. Zhang, C. Tian, J. Ou and J. Mi, Preparation of ceramsite from lead-zinc tailings and coal gangue: Physical properties and solidification of heavy metals, *Constr. Build. Mater.*, 2023, **368**, 130426.

34 L. Luo, Y. Liu, M. Oeser, A. García Hernandez and P. Liu, Unraveling the nano-cracking mechanism in aged asphalt binder with consideration of rejuvenation effects, *Eng. Fract. Mech.*, 2023, **292**, 109683.

35 Y. Gao, X. Liu, S. Ren, E. I. Assaf, P. Liu and Y. Zhang, Nanostructure and damage characterisation of bitumen under a low cycle strain-controlled fatigue load based on molecular simulations and rheological measurements, *Composites, Part B*, 2024, **275**, 111326.

36 L. W. Zhang, W. M. Ji and K. M. Liew, Mechanical properties of diamond nanothread reinforced polymer composites, *Carbon*, 2018, **132**, 232–240.

37 S. P. Patil, P. Shendye and B. Markert, Molecular dynamics simulations of silica aerogel nanocomposites reinforced by glass fibers, graphene sheets and carbon nanotubes: A comparison study on mechanical properties, *Composites, Part B*, 2020, **190**, 107884.

38 B. Cui and H. Wang, Molecular interaction of Asphalt-Aggregate interface modified by silane coupling agents at dry and wet conditions, *Appl. Surf. Sci.*, 2022, **572**, 151365.

39 D. D. Li and M. L. Greenfield, Chemical compositions of improved model asphalt systems for molecular simulations, *Fuel*, 2014, **115**, 347–356.

40 O. C. Mullins, The modified Yen model, *Energy Fuels*, 2010, **24**, 2179–2207.

41 M. P. Koopmans, J. W. De Leeuw, M. D. Lewan and J. S. Sinninghe Damste, Impact of dia- and catagenesis on sulphur and oxygen sequestration of biomarkers as revealed by artificial maturation of an immature sedimentary rock, *Org. Geochem.*, 1996, **25**, 391–426.

42 X. Lu, B. Kalman and P. Redelius, A new test method for determination of wax content in crude oils, residues and bitumens, *Fuel*, 2008, **87**, 1543–1551.

43 B. Cui, X. Gu, D. Hu and Q. Dong, A multiphysics evaluation of the rejuvenator effects on aged asphalt using molecular dynamics simulations, *J. Cleaner Prod.*, 2020, **259**, 120629.

44 M. Olbrich, P. Mayer and D. Trauner, A step toward polytwistane: synthesis and characterization of C_2-symmetric tritwistane, *Org. Biomol. Chem.*, 2014, **12**, 108–112.

45 X. Li, T. Wang, P. Duan, M. Baldini, H.-T. Huang, B. Chen, S. J. Juhl, D. Koeplinger, V. H. Crespi, K. Schmidt-Rohr, R. Hoffmann, N. Alem, M. Guthrie, X. Zhang and J. V. Badding, Carbon Nitride Nanothread Crystals Derived from Pyridine, *J. Am. Chem. Soc.*, 2018, **140**, 4969–4972.

46 S. Liu, H. Wang, J. Yang, S. Luo, Y. Liu, W. Huang, J. Hu, G. Xu and Z. Min, Force field benchmark of asphalt materials: Density, viscosity, glass transition temperature, diffusion coefficient, cohesive energy density and molecular structures, *J. Mol. Liq.*, 2024, **398**, 124166.

47 H. Zhang, J. Cao, H. Duan, H. Luo and X. Liu, Molecular dynamics insight into the adsorption and distribution of bitumen subfractions on Na-montmorillonite surface, *Fuel*, 2022, **310**, 122380.

48 M. Zhang, Y. Yu, Y. Luan, H. Zhou, X. Peng, L. Gong and H. Zhou, Effects of CNT microstructural characteristics on the interfacial enhancement mechanism of carbon fiber reinforced epoxy composites via molecular dynamics simulations, *Thin-Walled Struct.*, 2024, **195**, 111413.

49 Y. Pang, L. Sun, H. Zhan, X. Zheng, J. Zhang, C. Bian and C. Lü, Assessing the impact of ultra-thin diamond nanothreads on the glass transition temperature of a bituminous binder, *Nanoscale Adv.*, 2023, **5**, 6724–6735.

50 W. Jian, D. Hui and D. Lau, Nanoengineering in biomedicine: Current development and future perspectives, *Nanotechnol. Rev.*, 2020, **9**, 700–715.

51 B. Hess, Determining the shear viscosity of model liquids from molecular dynamics simulations, *J. Chem. Phys.*, 2002, **116**, 209–217.

52 F. Khabaz and R. Khare, Glass transition and molecular mobility in Styrene-Butadiene rubber modified asphalt, *J. Phys. Chem. B*, 2015, **119**, 14261–14269.

53 L. Luo, A. M. Awed, M. Oeser and P. Liu, Mechanisms of interfacial load transfer in the fracture process of carbon nanotube-reinforced bitumen composites, *Eng. Fract. Mech.*, 2023, **290**, 109521.

54 M. Bursch, J. M. Mewes, A. Hansen and S. Grimme, Best-Practice DFT Protocols for Basic Molecular Computational Chemistry, *Angew. Chem., Int. Ed.*, 2022, **61**, e202205735.

55 J. Ge, H. Yu, G. Qian, W. Dai, C. Zhang, C. Shi, H. Zhou, T. Nian and Y. Zhong, Enhancement mechanism of aggregate surface roughness structure on interfacial properties of asphalt mixtures, *Constr. Build. Mater.*, 2024, **449**, 138388.

56 G. Xu and H. Wang, Molecular dynamics study of oxidative aging effect on asphalt binder properties, *Fuel*, 2017, **188**, 1–10.

57 L. Zhang and M. L. Greenfield, Rotational relaxation times of individual compounds within simulations of molecular asphalt models, *J. Chem. Phys.*, 2010, **132**, 18.

58 Y. Huang, Z. Wu, L. Liang, J. Ying, L. Gui, P. K. Shen and Z. Q. Tian, Revealing the dependance of mechanical properties of asphalt binder on graphene size via multi-scale methods, *Mater. Des.*, 2023, **236**, 112478.

59 A. P. Thompson, H. M. Aktulga, R. Berger, D. S. Bolintineanu, W. M. Brown, P. S. Crozier, P. J. in 't Veld, A. Kohlmeyer, S. G. Moore, T. D. Nguyen, R. Shan, M. J. Stevens, J. Tranchida, C. Trott and S. J. Plimpton, LAMMPS - a flexible simulation tool for particle-based materials modeling at the atomic, meso, and continuum scales, *Comput. Phys. Commun.*, 2022, **271**, 108171.

60 F. Nie, W. Jian and D. Lau, An atomistic study on the thermomechanical properties of graphene and functionalized

Open Access Article. Published on 28 October 2025. Downloaded on 5/1/2026 11:16:17 PM.
This article is licensed under a Creative Commons Attribution-NonCommercial 3.0 Unported Licence.

graphene sheets modified asphalt, *Carbon*, 2021, **182**, 615–627.

61 P. Dauber-Osguthorpe, V. A. Roberts, D. J. Osguthorpe, J. Wolff, M. Genest and A. T. Hagler, Structure and energetics of ligand binding to proteins: *Escherichia coli*, dihydrofolate reductase trimethoprim, a drug-receptor system, *Proteins*, 1988, **4**, 31–47.

62 S. Plimpton, Fast parallel algorithms for short-range molecular dynamics, *J. Comput. Phys.*, 1995, **117**, 1–19.

This journal is © The Royal Society of Chemistry 2025